# RESEARCH ON OPTIMIZATION OF VIBRATION EAR PICKING PARAMETERS BASED ON CORN PLANT VIBRATION RESPONSE CHARACTERISTICS AND FINITE ELEMENT ANALYSIS

/

# 基于玉米植株振动响应特性与有限元分析的激振摘穗参数优化研究

**Pengxuan GUAN[1,2,3], Yipeng CUI[1,2,3], Jianning YIN[1,2,3], Zehao ZHA[1,2,3], Qiming YU[1,2,3], Duanyang GENG[1,2,3*)]**

[1)] College of Agricultural Engineering and Food Science, Shandong University of Technology, Zibo 255000, China;

[2)] Institute of Modern Agricultural Equipment, Shandong University of Technology, Zibo255091, China

[3)] Shandong Provincial Key Laboratory of Smart Agricultural Technology and Intelligent Agricultural Machinery and Equipment for Field Crops, Shandong University of Technology, Zibo255091, China;

*Tel: +86-13668641238; E-mail: dygxt@sdut.edu.cn*

*DOI: https://doi.org/10.35633/inmateh-76-83*

**Keywords:** *Finite element analysis; Vibration ear-picking; Vibration characteristics; Maize plant*

## ABSTRACT

*To reduce maize ear damage caused by ear-picking rollers during maize harvesting and to improve ear-picking efficiency, this study investigates the vibration response characteristics of maize plants and conducts comprehensive experimental research. Current research on vibration ear-picking predominantly conducts on the structural design and parameter optimization of ear-picking mechanisms, with comparatively limited attention given to the dynamic response patterns of maize plants under vibrational excitation. Therefore, it is essential to conduct an in-depth investigation into the mechanical behavior and vibration response characteristics of maize plants during the maize ear detachment process. In this study, the mechanical behavior of ear-bearing maize plants during the vibration ear-picking process was first analyzed, and a theoretical model was established. The optimal acceleration range for low-damage and high-efficiency ear-plant separation was identified, and the key parameters affecting ear-picking performance—namely amplitude, frequency, and clamping position—were determined. Based on the slope algorithm and response surface methodology, combined with finite element analysis, this study quantitatively evaluates the influence of various vibration parameters on the acceleration score $S_z$ at the ear-bearing region. A predictive model was established using a Box-Behnken experimental design, identifying the optimal parameter combination as an amplitude of 8 mm, a frequency of 18 Hz, and a clamping position of 106 mm. This model enables the quantitative analysis of excitation forces acting on the ear during the ear-picking process and provides a theoretical foundation for optimizing the structure of the excitation waveform, thereby offering valuable guidance for the subsequent optimization and design of vibration ear-picking systems.*

## 摘要

*为了减少玉米收获过程摘穗辊对果穗的啃伤，提升摘穗效果，本研究以玉米植株的振动响应特性为切入点，开展了相关试验研究。当前关于激振摘穗的研究多聚焦于摘穗机构结构与参数优化，而对玉米植株在激振条件下的动力学响应规律关注较少，故需深入探讨玉米植株在果穗分离过程中的力学行为变化规则与振动响应特性。本研究首先分析了激振摘穗过程中带穗植株的力学行为变化规则，建立了理论模型，明确了果穗-植株分离低损高效分离的加速度范围，确定了影响摘穗效果的关键参数：振幅、频率和夹持位置。基于斜率算法与响应面法，结合有限元分析，量化分析了不同激振参数对结穗处加速度得分 $S_z$ 的影响。根据 Box-Behnken 设计试验建立预测模型，确定最优参数组合为振幅 8mm、频率 18hz、夹持位置 106mm。该模型能定量分析摘穗过程中果穗的激振力，用于优化激振波结构，为后续激振摘穗的优化设计提供理论指导。*

## INTRODUCTION

Maize harvesting is a critical stage in the production process, and the quality of harvesting directly affects both the yield and the quality of maize *(Jun et al., 2024; Shulun et al. 2024)*. Maize ear damage not only affects the appearance quality of maize but also leads to yield reduction due to physical injury and increases the risk of mold growth during storage, thus becoming a major bottleneck that limits improvements in harvest quality *(Qihuan et al., 2025; Shulun et al., 2024)*. Therefore, reducing ear damage has become a critical measure for enhancing maize harvest quality.

To address the issue of maize ear damage caused by ear-picking rollers during the harvesting process, expert scholars have conducted extensive research *(Qiankun et al., 2020; Shanglong et al., 2023)*. For example, Tong Jin employed a bionic ear-picking roller combined with differential loading, which altered the loading direction and contact area during the ear-stalk separation process, thereby reducing maize ear damage during harvesting *(Feng, 2007)*. Hongyu Yan developed a vertical roller maize ear-picking technology, which allows the detached maize ears to leave the ear-picking rollers and thereby prevents secondary damage to the maize ears, effectively improving the overall harvest quality of maize *(Hongyu et al., 2009)*. Building upon the foundation of vertical roller ear-picking technology, our research team has developed a vibration ear-picking technique, in which high-frequency vibrations are applied to the maize stalk during the clamping and conveying process to achieve ear-stalk separation *(Xiaoqi et al., 2020)*. This approach avoids direct contact between the maize ear and the picking mechanism, effectively reducing maize ear damage, and has been successfully promoted and applied in companies such as Shandong DIMA and Jindafeng. However, it has been observed in practical production that excessive inertial force applied to the maize ear can result in premature breakage of maize plants and, in severe cases, lead to header blockages *(Wenxue et al., 2024; Ranbing et al., 2021)*. Conversely, insufficient inertial force may cause difficulties in separating the maize ear from the plant, thereby hindering the effectiveness of vibration ear-picking *(Zhang et al., 2022)*.Therefore, to improve ear-picking performance, it is necessary to accurately understand the variation of inertial forces acting on the maize ear during the vibration process and their relationship with operational parameters. Given that these inertial forces are directly dependent on the vibration response characteristics of maize plants under vibrational excitation, conducting research on the dynamic behavior of maize plants in such conditions is of great significance for revealing the mechanism of vibration ear-picking and guiding parameter optimization to enhance harvest efficiency and quality.

The separation of the maize ear from the plant during the vibration ear-picking process can be described as occurring when the inertial force generated by the acceleration of the maize ear exceeds the bonding force between the maize ear and the peduncle, thereby enabling effective detachment of the maize ear from the plant. Current research on vibration ear-picking primarily focuses on the structural design and parameter optimization of the ear-picking mechanism, while the dynamic response patterns of maize plants under vibrational excitation have received comparatively little attention *(Xiaoqi et al., 2020)*. This is mainly due to the complexity of effective excitation force transmission and the dynamic response characteristics of the plant, making it difficult to accurately capture the response patterns of maize plants using conventional experimental methods alone. To address this issue, the finite element analysis method provides an effective means of simulating the response patterns of maize plants to various excitation parameters. In recent years, this method, owing to its outstanding capability in simulating the dynamic behavior of complex structures, has been widely applied to the study of vibration responses and mechanical harvesting processes in agricultural and forestry crops *(Pereira et al., 2025; Delin et al., 2022)*. Longsheng Fu utilized finite element analysis software to investigate the vibration-based harvesting mechanism of sea buckthorn *(Longsheng et al., 2016)*. Guofeng Zhang optimized the vibration parameters for the mechanical harvesting of camellia fruit by integrating finite element analysis with dynamic modeling *(Kaizhan et al., 2019)*. Linyun Xu employed the finite element method to study the effects of ginkgo canopy structure on vibration response characteristics *(Xuan et al., 2021)*. However, finite element analysis studies focusing on the dynamic response patterns of maize plants under vibrational excitation remain limited.

In summary, although vibration ear-picking technology has already been applied in production, issues such as plant breakage and header blockages persist. Therefore, it is essential to further analyze the vibration response characteristics of maize plants and optimize the key parameters of the vibration ear-picking process. In this study, a theoretical analysis of the vibration ear-picking process was initially conducted to identify the key parameters influencing ear harvest quality and efficiency. Subsequently, finite element simulation software was utilized to numerically investigate the vibration response characteristics of maize plants, thereby determining the optimal ranges of critical operational parameters. Finally, an orthogonal experiment was performed to establish the optimal parameter combination, which was further validated through bench testing, confirming the accuracy and practical applicability of the research findings.

## MATERIALS AND METHODS

### Working Principle of Vibration Ear-Picking

#### The Overall Structure

As shown in Fig. 1(a), the vibration ear-picking header primarily consists of a crop divider, crop press

bar, ear-picking mechanism, conveyor belt, gathering chain and cutter bar. Its core component is the ear-picking roller assembly, which features symmetrically shaped, non-equilateral polygonal rollers (non-equilateral octagonal rollers), as shown in Fig. 1(b). During operation, ear-bearing maize plants are conveyed rearward under the clamping action of the rotating ear-picking roller assembly. In this process, the irregular polygonal edges of the rollers impart periodic excitation forces to the ear-bearing maize plants, inducing high-frequency lateral oscillations, as illustrated in Fig. 1(c).During the reciprocating oscillation, when the inertial force exerted on the maize ear exceeds the bonding force between the maize ear and the peduncle, the maize ear is separated from the stalk, thereby achieving effective detachment of the maize ear from the plant, as shown in Fig. 1(d).

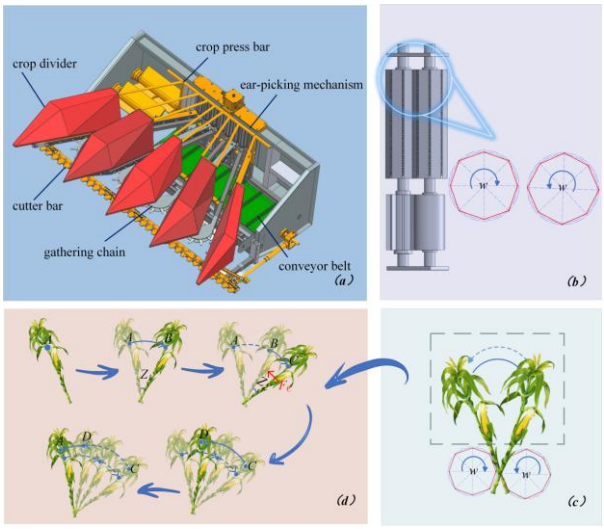


**Fig. 1 - Schematic diagrams of harvesting principle**

*(a) the vibration ear-picking header; (b) the ear-picking mechanism; (c) the geometry and working principle of the ear-picking roller; and (d) the movement of the maize plant (the solid line represents the displacement during forward travel, while the dashed line denotes the displacement at the corresponding step).*

**Theoretical Model**

Fig. 1(d) presents a complete cycle of the reciprocating motion of the maize plant during the vibration ear-picking process. Under the action of the ear-picking rollers, the ear-bearing plant undergoes simple harmonic vibration, which can be described by the following kinematic equation:

$$\theta = Z\sin(\omega t + \phi) \tag{1}$$

Under the influence of the excitation waveform, the ear-bearing maize plant accelerates from point A to point B. When the direction of vibration reverses, the velocity of the maize ear rapidly drops to zero due to inertia, and the plant moves from point B to point C. The process from point C to point D and back to point A is the exact reverse of the previous motion. Since the motion is symmetrical within a single cycle, only the dynamics within a half-cycle are analyzed.

Since the angle of motion differs during the acceleration and deceleration phases, when the maize ear is initially at rest, the equation of motion for the maize ear during the phase from A to B is as follows:

$$\theta_{AB} = Z_1\sin(\omega_1 t) \tag{2}$$

where, $\theta_{AB}$ is the angular displacement of the maize ear from point A to point B, $Z_1$ is the maximum angular amplitude during this phase, and $w_1$ is the angular velocity during the acceleration from A to B. The equation of motion for the maize ear during the phase from point B to point C is as follows:

$$\theta_{BC} = Z2\sin\left[\omega_2\left(t - \frac{\pi}{2\omega_1}\right)\right] \tag{3}$$

where, $\theta_{BC}$ is the angular displacement of the maize ear from point B to point C, $Z_2$ is the maximum angular amplitude during this phase, and $w_2$ is the angular frequency during the rapid attenuation phase from B to C.

According to the Eq. (1), the angular acceleration of the maize ear is given by:

$$\varepsilon = \frac{d\theta}{dt} = \omega Z\cos(\omega t + \phi) \tag{4}$$

Therefore, the maximum angular acceleration of the maize ear is:

$$\varepsilon_{\max} = \omega Z \tag{5}$$

According to the theorem of simple harmonic motion, acceleration attains its maximum value at the endpoints. Specifically, at point C, the maximum acceleration is acting on the maize ear. The maximum acceleration of the maize ear is:

$$a_{\max} = r\varepsilon_{\max} = r\omega_2 Z2 \quad (6)$$

Let $\beta$ be defined as the ratio of the angular amplitude $Z_2$ during the deceleration phase to the total angular amplitude $Z$ from point A to point C, as expressed by:

$$\beta = \frac{Z2}{Z} \quad (7)$$

When the motion period T = 2π/ω=1/f, according to Eq. (6), the maximum acceleration of the maize ear, $a_{max}$, can be expressed as:

$$a_{\max} = 2\pi \mathrm{r}\, fZ\beta \quad (8)$$

where, $r$ is the distance from the clamping position to the maize ear, $f$ is the vibration frequency of the ear-bearing plant, $Z$ is the angular amplitude of the maize ear from point A to point C, and $\beta$ is the ratio of the angular amplitude $Z_2$ during the deceleration phase to the total angular amplitude $Z$ from point A to point C.

According to Newton's second law and Eq. (8), the maximum force acting on the maize ear during the motion is given by:

$$F_C = ma_{\max} = 2\pi \,\mathrm{r}\, m\, f\, Z\, \beta \quad (9)$$

where $m$ is the mass of the maize ear, $\beta$ is the ratio of the angular amplitude $Z_2$ during the deceleration phase to the total angular amplitude $Z$ from point A to point C, $Z$ is the angular amplitude of the maize ear from point A to point C, $f$ is the vibration frequency of the ear-bearing plant, and $r$ is the distance from the clamping position to the maize ear.

Based on the above theoretical analysis, it can be concluded that the primary factors influencing the excitation force are the vibration frequency $f$, the vibration amplitude $Z$, and the clamping position $r$.

## Development of a Simplified Maize Plant Model

### Material Properties of the Maize Plant

To investigate the vibration response characteristics of maize plants, the physical parameters of the plants were measured. In this study, the widely cultivated maize variety "Xianyu 335" from Shandong Province was selected as the experimental subject.

The measurement methods were as follows: the instruments used included a tape measure, ruler, vernier caliper, high-precision electronic balance, push-pull force gauge, and texture analyzer. The measured parameters encompassed the fundamental structural characteristics of the maize plant and the maize ear, including plant height, stem diameter, plant breaking force, ear-bearing height, maize ear mass, and peduncle bonding force.

**Table 1**

**Physical Parameters of the Maize Plant**

| | Plant height (mm) | Stem Diameter (mm) | Breaking Force (N) | Ear-Bearing Height (mm) | Maize Ear Mass (g) | Peduncle Bonding Force (N) |
|---|---|---|---|---|---|---|
| Min | 2495 | 19.2 | 89 | 975 | 205 | 48 |
| Max | 2663 | 21.4 | 136 | 1035 | 263 | 60 |
| Mean | 2500.42 | 20.24 | 103.5 | 1026.56 | 243.39 | 53.5 |

### Measurement of Material Properties

The density of maize plants was determined using the water displacement method *(Zijie et al., 2022)*. Specifically, the plant volume was measured by displacement, and the mass was measured using an electronic balance with a precision of 0.01 g. The density was then calculated as the ratio of mass to volume. To improve measurement accuracy, the collected plant samples were divided into ten groups, with the volume and corresponding mass of each group measured separately. The average value of the calculated densities was taken, resulting in an average density of 1003 kg/m³.

To determine additional engineering parameters of the maize plant, the de-eared plant was simplified as a cylindrical structure. The center of the cylinder's base was defined as the origin of the coordinate system, with the base lying on the X-Y plane and the plant's axial direction aligned with the Z-axis, thereby constructing a geometric model of the plant in the X-Y-Z coordinate system. In this model, it was assumed that the material was uniformly distributed and exhibited consistent mechanical properties throughout.

Thus, the simplified maize plant could be regarded as an orthotropic material, characterized by nine engineering parameters: the radial elastic modulus $E_x$ and $E_y$, axial elastic modulus $E_z$, radial shear modulus $G_{yz}$ and $G_{xz}$, axial shear modulus $G_{xy}$, Poisson's ratio $\beta_{xy}$, $\beta_{yz}$ and $\beta_{xz}$), and the relationship for the engineering parameters of orthotropic materials is expressed using Eq. (10)

$$\begin{cases} E_x = E_y \\ G_{yz} = G_{xz} \\ \beta_{yz} = \beta_{xz} \\ G_{xy} = \dfrac{E_x}{2(1+\beta_{xy})} \end{cases} \tag{10}$$

To obtain the engineering parameters of the maize plant, compression and three-point bending tests were conducted using a texture analyzer (Fig. 2), with the compression and bending head speeds controlled at 3 mm/s and 5 mm/s, respectively.

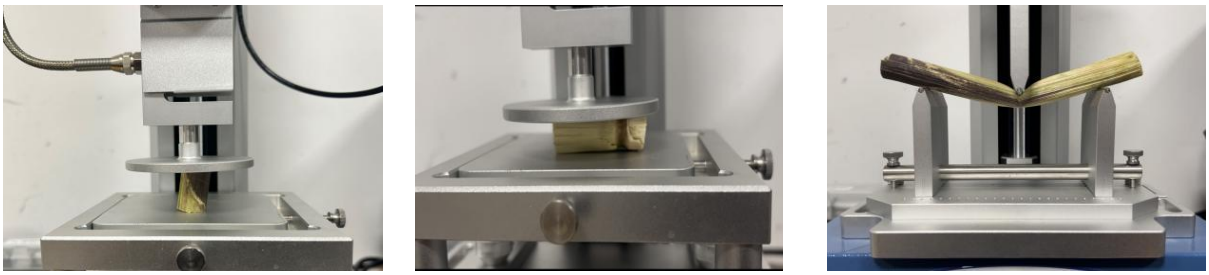

（a） （b） （c）

**Fig. 2 - Measurement of engineering parameters using a texture analyzer**

According to the reference *(Jian et al., 2021)*, the elastic modulus of the sample can be calculated as follows:

The compressive stress of the tested material is calculated as:

$$\sigma = \frac{F}{A_0} \tag{11}$$

The strain equation of the tested material is given by:

$$\varepsilon = \frac{\Delta l}{l_0} \tag{12}$$

Thus, the elastic modulus of the tested material is:

$$E = \frac{\sigma}{\varepsilon} = \frac{F}{\Delta l} \cdot \frac{l_0}{A_0} = \frac{k \cdot l_0}{A_0} \tag{13}$$

where $F$ is the applied load (N), $A_o$ is the cross-sectional area of the plant (mm$^2$), $\sigma$ is the stress (MPa), $\varepsilon$ is the strain, $\Delta l$ is the deformation length(mm), $l_o$ is the initial length of the sample(mm), and $k$ is the slope of the load-displacement curve (N/mm).

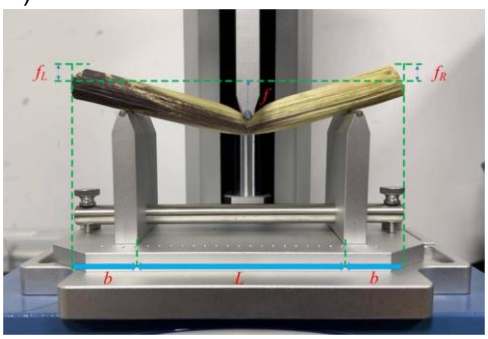


**Fig. 3 - Schematic diagram of the three-point bending shear test and parameter annotations.**

The three-point bending test was used to calculate the radial shear modulus (Fig. 3) *(Jian et al., 2021)*. The radial shear modulus of the sample can be determined using Eq. s (15) to (16).

$$f_1 = \frac{f_L + f_R}{2} \quad (14)$$

$$H = \frac{\Delta p \cdot L^4}{f - \frac{f_1 \cdot L^3}{b}} \quad (15)$$

$$G_{yz} = \frac{4H}{\pi D^2} \quad (16)$$

Where $\triangle p$ is the load increment during the elastic deformation stage (N); $f_i$ is the extension deviation increment (mm); $L$ is the span between the supports (mm); $b$ is the extension length (mm); $f$ is the midspan deflection increment (mm); $H$ is the shear stiffness (N/mm); $D$ is the diameter of the tested sample (mm) and $f_L$ and $f_R$ are the extension deflection increments on the left and right sides, respectively (mm).

According to the relevant literature, the Poisson's ratio $\beta_{xy}$ of the isotropic plane is defined as 0.3 (*Zhouzhou et al., 2024*). The relationship between the Poisson's ratio $\beta_{xy}$ of the isotropic plane and the Poisson's ratio $\beta_{yz}$ of the orthotropic plane is expressed by Eq. (17).

$$\beta_{yz} < \frac{1}{2} \cdot \beta_{xy} \cdot \frac{E_x}{E_z} \quad (17)$$

Although most existing studies treat maize stalks as having identical material properties, this approach may not be sufficiently accurate for the present study and could compromise the reliability of the simulation results. Therefore, axial compression, radial compression, and three-point bending shear tests were conducted on maize plants (Fig.2). Based on the aforementioned measurement methods, the nine engineering parameters required for simulation were calculated, as summarized in Table 2.

**Table2**

**Material Property Parameters of the Maize Plant**

| $E_x$/MPa | $E_y$/MPa | $E_z$/MPa | $G_{xy}$/MPa | $G_{xz}$/MPa | $G_{yz}$/MPa | $\beta_{xy}$ | $\beta_{xz}$ | $\beta_{yz}$ | ρ(kg/m$^3$) |
|---|---|---|---|---|---|---|---|---|---|
| 373.58 | 373.58 | 5773.6 | 145.5 | 2886.8 | 2886.8 | 0.3 | 0.019 | 0.019 | 1003 |

**Vibration Response Simulation**

To determine the acceleration response of the maize ear under specific operating conditions, this study employed 3D modeling software and finite element analysis software (SolidWorks/Ansys) to conduct numerical simulations of the vibration response characteristics of maize plants. Specifically, a geometric model of the maize plant was first created using SolidWorks, and the relevant structural parameters were subsequently imported into Ansys for dynamic simulation analysis, thereby obtaining the vibration response characteristics of the maize stalk.

In this study, finite element analysis software (*Ansys Workbench, 2021-R1*) was used to perform dynamic simulations in order to replicate the kinematic behavior of actual maize plants under identical conditions. During the simulation process, the maize plant model was first established in SolidWorks (2020) based on the average geometric dimensions provided in Table1. Subsequently, the model was imported into the finite element analysis software for mesh generation, with the element size set to 10 mm, and the material properties obtained from Table 2 were assigned to the model accordingly. Since the excitation force is transmitted to the maize ear through the plant, this study focuses solely on analyzing the vibration acceleration at the measurement points near the ear-bearing position. Considering the inherent variability in maize ear-bearing height, to enhance the accuracy of the simulation results, seven measurement points were evenly distributed along the plant's axial direction at 10 mm intervals around the ear-bearing region. The response acceleration at each measurement point was extracted using acceleration probes in the post-processing module, as shown in Fig. 4.

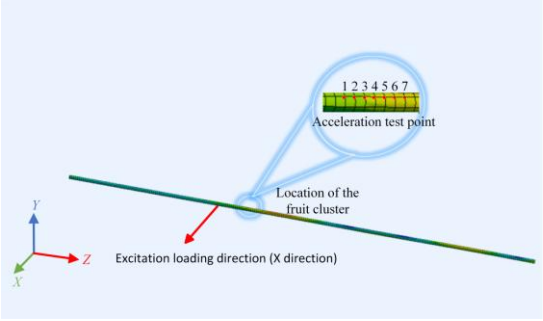


**Fig. 4 - Simulation model of the maize plant and distribution of measurement points**

The simulation conditions illustrated in Figure 4 are as follows: to study the effect of different clamping positions on the acceleration response at the ear-bearing region, the excitation amplitude and frequency were kept constant while only the position of the applied vibration load was varied, thereby analyzing the relationship between clamping position and acceleration response. When investigating the effects of different amplitudes and frequencies on the acceleration response at the ear-bearing region, the clamping position was fixed. The excitation amplitude and frequency were adjusted by modifying the displacement and frequency settings in the harmonic response analysis module. A periodic sinusoidal excitation force was applied along the X-axis to the clamping region of the plant model. The acceleration responses at the ear-bearing region under various amplitudes and frequencies were then obtained, allowing the identification of the variation patterns between excitation frequency, amplitude, and acceleration response.

To evaluate the inertial forces acting on the maize ear under different excitation parameters and their effects on the separation performance, the harmonic response analysis module was employed to simulate the acceleration response characteristics of the maize plant under various combinations of excitation parameters. Based on the degree of influence of each parameter on maize ear–stalk separation, amplitude, frequency, and clamping position were selected as the experimental factors to investigate their effects on the acceleration score index $Sz$. For amplitude, if it is too small, the resulting acceleration may be insufficient to achieve maize ear–stalk separation; conversely, an excessively large amplitude may cause premature breakage of the maize plant. Based on relevant studies *(Duanayng et al., 2019)*, the amplitude range was selected between 5 mm and 15 mm. For frequency, excessively low values may result in an insignificant excitation effect, while excessively high values could induce maize plant fatigue failure. Based on relevant studies *(Duanyang et al., 2017)*, the frequency range was set between 16 Hz and 20 Hz. The clamping position was optimized within the range of 50 mm to 170 mm based on the team's previous research *(Qian et al., 2018)*. The levels of the experimental factors are shown in Table 2.

**Table 2**

**Factors and levels of experiment**

| Level | Factor | | |
|---|---|---|---|
| | Amplitude (mm) | Frequency (Hz) | Clamping position (mm) |
| 1 | 5 | 16 | 50 |
| 2 | 7.5 | 17 | 80 |
| 3 | 10 | 18 | 110 |
| 4 | 12.5 | 19 | 140 |
| 5 | 15 | 20 | 170 |

This section established an accurate finite element model of the maize plant based on its actual geometric structure and material properties. Harmonic response analysis was conducted to simulate the acceleration characteristics of the ear-bearing region under varying amplitude, frequency, and clamping position. The results provide essential data support for the subsequent development of an evaluation index system centered on ear acceleration.

**Evaluation Index**

Considering that insufficient acceleration of the maize ear under excitation may hinder effective ear-stalk separation, while excessive acceleration may lead to premature plant breakage-resulting not only in the failure of ear-stalk separation but also in potential header blockages—it is essential to optimize the vibration parameters for the ear-picking process. Given that the elastic modulus calculation in Eq. (13) involves the load-displacement slope k, a slope-based scoring algorithm was introduced to evaluate and rank the acceleration at each measurement point *(Peng et al., 2022)*. In this study, the vibration acceleration at the measurement points near the ear-bearing region was quantified using the scoring method, and the average acceleration score S, across all points was adopted as the evaluation index. Specifically, the difference between the acceleration at each measurement point and the critical acceleration $a_{min}$ (the minimum acceleration required for ear-stalk separation) was used as the basis for determining the score at each measurement point.

Assuming the acceleration required for ear-stalk separation is ai, the acceleration range for ear-stalk separation can be expressed by Eq. (18):

$$\frac{f_a}{m} \le a_i \le \frac{f_b}{m} \tag{18}$$

where:

$m$ is the average mass of the maize ear; $f_a$ is the maximum peduncle bonding force (N);

$f_b$ is the minimum plant breaking force (N);

$a_i$ is the acceleration required for ear-stalk separation (m/s$^2$).

By substituting the data from Table1 into Eq. (16), the calculated acceleration range that satisfies ear-stalk separation without causing plant breakage is obtained as follows: the minimum acceleration $a_{min}$=246.52m/s$^2$ and the maximum acceleration $a_{max}$=365.67m/s$^2$.

The specific scoring criteria are illustrated in Fig. 5. For each measurement point near the ear-bearing region, the maximum score was set at 100 points. When the acceleration at a measurement point equals $a_{min}$, it is considered optimal—achieving ear-stalk separation without causing premature plant breakage—and thus the score for that point is defined as 100 points. If the acceleration is less than $a_{min}$, the score is assigned as O points. If the acceleration exceeds $a_{min}$, the score is proportionally reduced based on the degree of exceedance. The average score $S_z$, across all measurement points is used as the evaluation index to assess the overall vibration effect. The score for each measurement points within the ear-bearing region and the average score $S_z$, can be calculated using Eq. s (19)-(20), respectively, as follows:

$$S_i = 100 - \frac{(a_i - a_{\min})}{a_{\max} - a_{\min}} \times 100 \quad (19)$$

The vibration acceleration score at each measurement point within the ear-bearing region is calculated according to Eq. (19), and the average score across all measurement points can be expressed as:

$$S_z = \frac{1}{n}\sum_{i=1}^{n} S_i \quad (20)$$

where:

$S_i$ — score of an individual measurement point;

$S_z$ — average score of all measurement points;

$a_{max}$ — maximum allowable separation acceleration (m/s²);

$a_i$ — acceleration at the measurement point to be scored (m/s²);

$a_{min}$ — minimum required separation acceleration (m/s²).

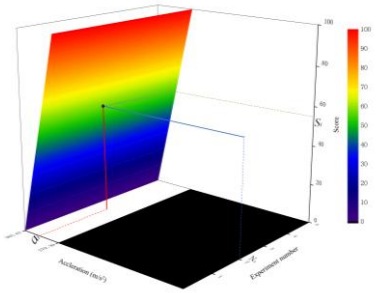

**Fig. 5 - Schematic diagram of the slope-based scoring algorithm**

**Bench verification test**

The effectiveness of the optimized parameter combination was verified using an image acquisition platform specifically constructed for the maize vibration ear-picking process. This platform consists of four main components: a test bench, a high-speed camera (X150, Revealer Company), a computer, and a fill light (EF-200, Shanghai Jinbei Company), as shown in Fig. 6. The test bench primarily includes a motor (Model: YE2-100L-2, speed range: 0–2870 r/min), a frequency converter, an ear-picking mechanism, a gathering chain, a crop press plate, and a reciprocating cutter bar. The motor provides the power source for the ear-picking rollers while simultaneously driving the gathering chain.

During the experiment, several maize plants of the "Xianyu 335" variety with similar ear-bearing heights were selected as test materials. To accurately capture the acceleration during ear–stalk separation, the high-speed camera was set to a frame rate of 1000 frames per second, an exposure time of 999 μs, and a resolution of 2560 × 1920 pixels. After starting the test bench, observations continued until the maize ear detached from the plant. The separation acceleration was analyzed using high-speed imaging analysis software (Revealer Company), and the acceleration score was evaluated based on the slope-based scoring algorithm. The experiment was repeated five times.

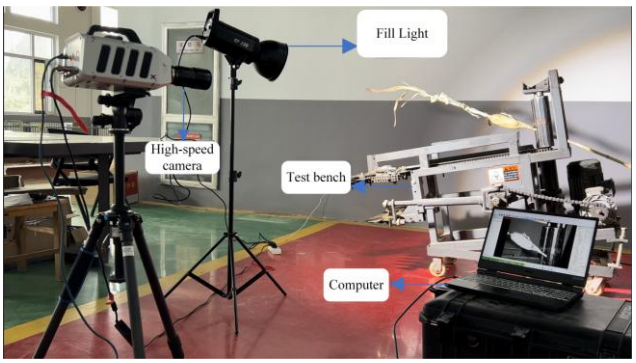


**Fig. 6 - Verification Test Setup**

## RESULTS

### Single-Factor Experimental Analysis

To determine the appropriate level ranges for the orthogonal experiment, single-factor tests were conducted based on the experimental method described in Section 2.4, using the average acceleration score $S_z$ as the performance evaluation criterion to investigate the influence patterns of each factor on the ear-picking performance.

### Influence of Amplitude on the Acceleration

The effect of amplitude on acceleration was obtained through experiments, as shown in Fig. 7. As illustrated in Fig. 7(b), the influence of amplitude on the average acceleration score $S_z$ exhibits a trend of first increasing and then decreasing. When the amplitude is less than 7.5 mm, the score $S_z$ increases with the increase in amplitude; however, when the amplitude exceeds 7.5 mm, the score $S_z$ decreases significantly. The underlying reason, as shown in Fig. 7(a), is that at lower amplitudes, the acceleration at some measurement points does not reach the acceleration scoring range, resulting in a lower $S_z$. As the amplitude increases to 7.5 mm, more measurement points achieve acceleration values within the scoring range, leading to an improvement in $S_z$ and reaching its peak. When the amplitude is further increased, the acceleration at some measurement points exceeds the upper limit of the scoring range, causing a decline in $S_z$. Considering these results, an amplitude range of 5–10 mm is deemed appropriate for the orthogonal experiment.

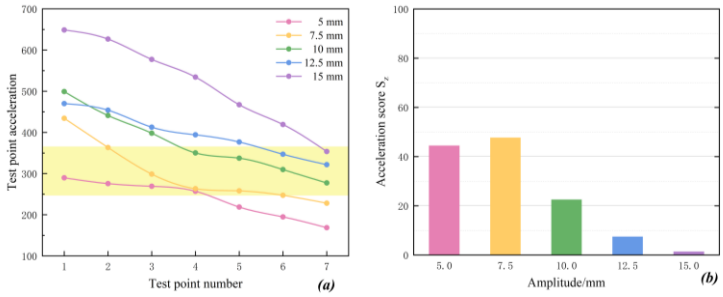


*Note: The yellow-shaded area represents the acceleration scoring range.*

**Fig. 7 - Experimental results for amplitude**

*(a) acceleration at each measurement point; (b) average acceleration score.*

### Influence of Frequency on the Acceleration

The effect of frequency on acceleration was obtained through experiments, as shown in Fig. 8. As illustrated in Fig. 8(b), the influence of frequency on the average acceleration score $S_z$ exhibits a trend of first increasing and then decreasing. When the frequency is below 17 Hz, the score $S_z$ increases with rising frequency; however, when the frequency exceeds 17 Hz, the score $S_z$ decreases as the frequency continues to increase. The underlying reason, as shown in Fig. 8(a), is that at lower frequencies, the excitation-induced acceleration is relatively low, causing some measurement points to fall below the acceleration scoring range and resulting in a lower $S_z$. As the frequency increases, more measurement points enter the acceleration scoring range, thereby leading to an increase in $S_z$. However, when the frequency further increases, the acceleration at some points significantly deviates from the scoring range, ultimately causing a decline in $S_z$. Considering these results, a frequency range of 17–19 Hz is considered appropriate for the orthogonal experiment.

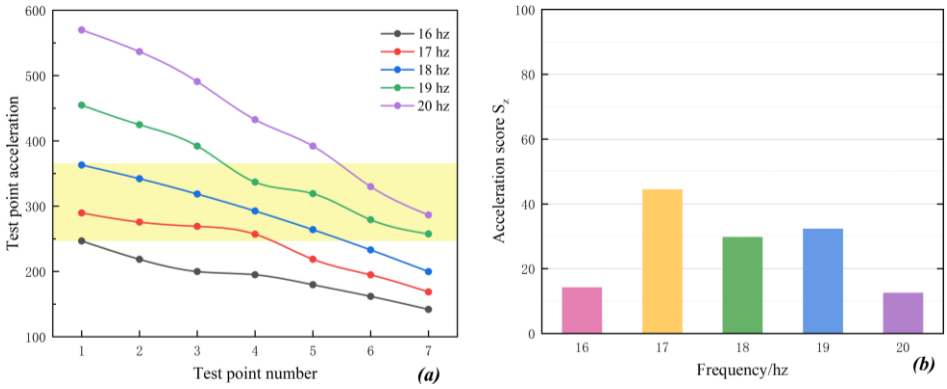


*Note: The yellow-shaded area represents the acceleration scoring range.*

**Fig. 8 - Experimental results for frequency**

*(a) acceleration at each measurement point; (b) average acceleration score.*

**Influence of clamping position on the Acceleration**

The effect of clamping position on acceleration was obtained through experiments, as shown in Fig. 9. As illustrated in Fig. 9(b), the influence of clamping position on the average acceleration score $S_z$ exhibits a trend of first increasing and then decreasing. When the clamping position is less than 80 mm, the score $S_z$ increases with increasing clamping distance; however, when the clamping position exceeds 80 mm, the score $S_z$ decreases with further increases in clamping distance. The underlying reason, as shown in Fig. 9(a), is that when the clamping position is too close to the maize ear, the transmitted acceleration in the ear-bearing region becomes excessively large, causing some measurement points to deviate significantly from the optimal acceleration $a_{min}$, thereby reducing the score $S_z$. Conversely, when the clamping position is too far, the propagation distance of the excitation wave increases, leading to a gradual reduction in acceleration at some points, eventually falling below the scoring range and resulting in a lower $S_z$. Considering these results, a clamping position range of 50–140 mm is considered appropriate for the orthogonal experiment.

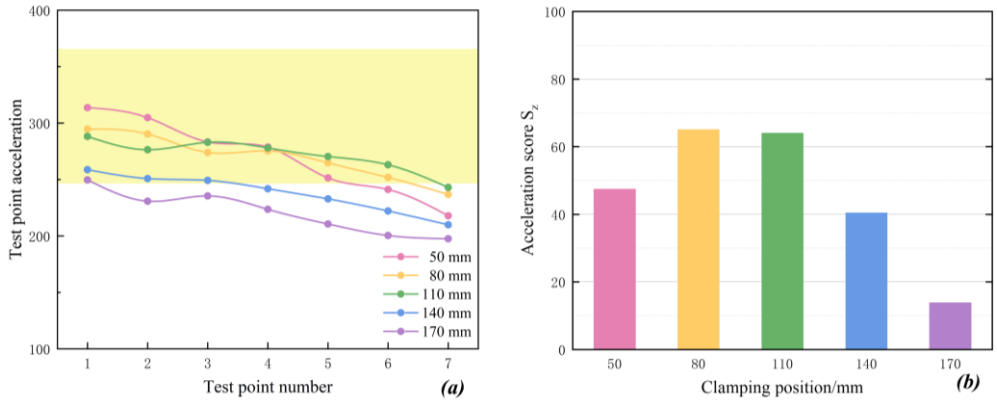


*Note: The yellow-shaded area represents the acceleration scoring range.*

**Fig. 9 - Experimental results for clamping position**

*(a) acceleration at each measurement point; (b) average acceleration score.*

Considering that vibration ear-picking relies on the combined effects of the three parameters to achieve maize ear–stalk separation, further optimization of the operating parameters is necessary to obtain the optimal parameter combination for the vibration ear-picking process.

**Optimal Parameter Combination**

To obtain the optimal operating parameters for vibration ear-picking, a three-factor, three-level orthogonal experiment was conducted on the three parameters that significantly affect the average acceleration score $S_z$. In this experiment, the average acceleration score $S_z$ was used as the performance evaluation index, with amplitude $X_1$, frequency $X_2$, and clamping position $X_3$ selected as the experimental factors. The test factors and their corresponding levels are listed in Table 3.

**Table 3**

**Factor Coding**

| Level | Amplitude $X_1$ (mm) | Frequency $X_2$ (Hz) | Clamping position $X_3$ (mm) |
|---|---|---|---|
| -1 | 5 | 17 | 50 |
| 0 | 7.5 | 18 | 95 |
| 1 | 10 | 19 | 140 |

The Box-Behnken experimental design method was used to determine 17 sets of simulation test results for vibration ear-picking. The simulation data were then subjected to second-order multiple regression analysis using Design Expert software to study the effects of amplitude, frequency, and clamping position on the test index $S_Z$ Ultimately, the optimal combination of vibration ear-picking parameters was determined.

**Table 4**

**Orthogonal Test Results**

| Test No. | Amplitude $X_1$ (mm) | Frequency $X_2$ (Hz) | Clamping Position $X_3$ (mm) | Average Acceleration Score $S_Z$ |
|---|---|---|---|---|
| 1 | 0 | 0 | 0 | 90.8 |
| 2 | -1 | -1 | 0 | 10.2 |
| 3 | -1 | 1 | 0 | 69.32 |
| 4 | 1 | 1 | 0 | 76.55 |
| 5 | -1 | 0 | 1 | 54.38 |
| 6 | 0 | 0 | 0 | 89.9 |
| 7 | 0 | -1 | -1 | 12.5 |
| 8 | 0 | 1 | -1 | 83.4 |
| 9 | 1 | 0 | 1 | 81.26 |
| 10 | 0 | 0 | 0 | 91.4 |
| 11 | 0 | 1 | 1 | 74.23 |
| 12 | 0 | 0 | 0 | 86.39 |
| 13 | 0 | 0 | 0 | 89.5 |
| 14 | 1 | 0 | -1 | 43.65 |
| 15 | -1 | 0 | -1 | 45.36 |
| 16 | 0 | -1 | 1 | 67.35 |
| 17 | 1 | -1 | 0 | 33.68 |

**Table 5**

**Analysis of Variance (ANOVA)**

| Source | Sum of squares | Degree of freedom | Mean square | *F*-value | *P*-value | significant level |
|---|---|---|---|---|---|---|
| Model | 11486.84 | 9 | 1276.32 | 96.80 | < 0.0001 | ** |
| $X_1$ | 390.32 | 1 | 390.32 | 29.60 | 0.0010 | * |
| $X_2$ | 4039.66 | 1 | 4039.66 | 306.37 | < 0.0001 | ** |
| $X_3$ | 1065.14 | 1 | 1065.14 | 80.78 | < 0.0001 | ** |
| $X_1X_2$ | 66.02 | 1 | 66.02 | 5.01 | 0.0603 | |
| $X_1X_3$ | 204.35 | 1 | 204.35 | 15.50 | 0.0056 | * |
| $X_2X_3$ | 1024.64 | 1 | 1024.64 | 77.71 | < 0.0001 | ** |
| $X_1^2$ | 2166.58 | 1 | 2166.58 | 164.32 | < 0.0001 | ** |
| $X_2^2$ | 1597.20 | 1 | 1597.20 | 121.13 | < 0.0001 | ** |
| $X_3^2$ | 486.71 | 1 | 486.71 | 36.91 | 0.0005 | * |
| Residual | 92.30 | 7 | 13.19 | | | |
| Lack of Fit | 77.21 | 3 | 25.74 | 6.83 | 0.0473 | |
| Pure Error | 15.08 | 4 | 3.77 | | | |
| Cor Total | 11579.14 | 16 | | | | |

*Note: P<0.01 (Highly significant), 0.01≤P<0.05 (Significant). ** indicates highly significant, * indicates significant.*

As shown in Table 5, for the $S_z$ model, P<0.0001 indicates that the quadratic multiple regression model is highly significant. The lack-of-fit term is not significant, suggesting that the experimental error is small and the regression equation fits the data well. In the average acceleration score model, $P$<0.01 for $X_2$, $X_3$, $X_2X_3$, $X_1^2$, and $X_2^2$ indicates that these factors have a highly significant effect on the regression model within a 99% confidence interval. From the analysis of the regression coefficients, the sequence of factor significance on the acceleration score model is: frequency, clamping position, and amplitude. For $X_1$, $X_1X_3$, and $X_3^2$, P<0.05 shows that their influence on the regression model is significant within a 95% confidence interval. Other terms have $P$ values greater than 0.05, indicating that their effect on the regression model is not significant. After eliminating the non-significant terms and performing variance fitting, the final multiple quadratic regression equation for the acceleration score $S_z$ is:

$$S_z = 89.60 + 6.98x_1 + 22.47x_2 + 11.54x_3 + 7.15x_1x_3 - 16.00x_2x_3 - 22.68x_1^2 - 19.48x_2^2 - 10.75x_3^2 \quad (21)$$

**Response Surface Analysis**

Figure 10a illustrates the response surface of frequency and amplitude. As both frequency and amplitude increase, the acceleration score $S_z$ initially rises and then declines. Interaction analysis reveals that under low frequency and small amplitude, the overall acceleration of the plant is insufficient, causing most test points to fall outside the scoring range, resulting in a low $S_z$. As frequency and amplitude increase, the acceleration values at various test points gradually enter the effective scoring range, leading to a sharp increase in $S_z$. However, when the excitation intensity becomes excessive, some test points exceed the scoring range, causing a reduction in $S_z$.

Figure 10b presents the response surface of amplitude and clamping position. As clamping position and amplitude increase, $S_z$ shows a rising trend followed by a decline. Interaction analysis indicates that increasing the clamping position extends the transmission distance, which reduces the acceleration transmitted to the maize ear. Conversely, increasing amplitude enhances the overall plant acceleration. Therefore, under the combined effect of both factors, a moderate clamping position and amplitude bring the acceleration near the critical threshold, resulting in an increased $S_z$.

Figure 10c depicts the response surface of frequency and clamping position. With increasing clamping position and frequency, $S_z$ rapidly increases and then stabilizes. Interaction analysis shows that at low frequency or short clamping distance, the acceleration often falls outside the scoring range, resulting in low $S_z$. As frequency increases or clamping distance moderately extends, more test points fall within the effective range, leading to a significant improvement in $S_z$. However, if frequency or clamping distance becomes too large, some test points again deviate from the scoring range, and $S_z$ growth slows.

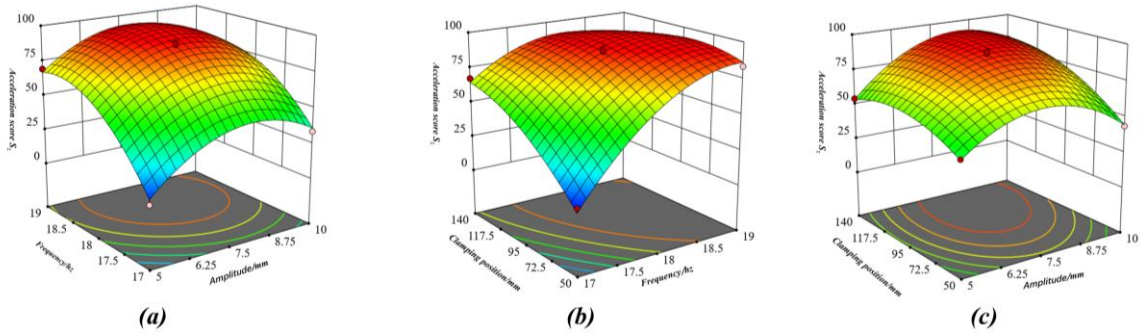


**Fig. 10 - Response Surface Analysis of Acceleration Score**

**Parameter Optimization and verification test**

Taking amplitude, frequency, and clamping position as optimization variables, the optimal parameter combination was determined using the average acceleration score $S_z$ as the evaluation index. The optimal combination for effective ear-picking was found to be an amplitude of 7.88 mm, a frequency of 18.46 Hz, and a clamping position of 105.94 mm, corresponding to an acceleration score $S_z$ of 96.71. To verify the reliability of the simulation results, the parameters were rounded to an amplitude of 8 mm, a frequency of 18 Hz, and a clamping position of 106 mm.

Bench tests were conducted five times using a self-developed image acquisition platform for vibration ear-picking of maize. The results showed a maximum score of 97.31, a minimum score of 90.68, and an average score of 93.61. The error between test and simulation results was 2.36%, confirming the predictive accuracy of the model and the practical applicability of the optimized parameters.

**Table 6**

**Verification Results of Bench Tests**

| Indicator | Minimum value | Maximum | Average value | SD | Error (%) |
|---|---|---|---|---|---|
| average acceleration score $S_z$ | 90.68 | 97.31 | 93.61 | 2.72 | 3.21 |

## CONCLUSIONS

Based on the finite element analysis method, simulation tests were conducted to analyze the acceleration amplitude response of maize plants under different excitation parameters. The ear-picking process and its main influencing factors were examined, and the reliability and accuracy of the simulation results were validated through bench tests. The main conclusions are as follows:

(1) By analyzing the changes in the mechanical behavior of maize plants during the ear-picking process, it was determined that the main factors influencing ear-picking performance are amplitude, frequency, and clamping position. This provides a theoretical foundation for subsequent analyses of the vibration response characteristics of maize plants.

(2) The vibration response characteristics of maize plants were explored, providing a basis for the calculation and prediction of the excitation forces acting on the maize ear under different working parameters.

(3) Single-factor tests for amplitude, frequency, and clamping position were conducted using simulation software to determine the influence of these three variables on the acceleration score. Furthermore, using these parameters as test factors, a three-factor, three-level orthogonal experiment and response surface analysis were carried out with acceleration score as the evaluation criterion. A slope-based scoring algorithm was employed to assist in decision-making. The optimal parameter combination was determined to be amplitude of 7.88 mm, frequency of 18.46 Hz, and clamping position of 105.94 mm, which yielded the best ear-picking performance. After rounding the optimal parameters and conducting verification tests, the average acceleration score $S_z$ was found to be 93.61, indicating that the verification test results closely matched the optimized regression prediction values. This confirmed the reliability of the simulation results and provided new insights for vibration ear-picking.

## ACKNOWLEDGEMENT

This work was supported financially by the National Natural Science Foundation of China under Grant No. 32372008.

## REFERENCES

[1] Chen, K., Du, X., Zhang, G., & Zhou, R. (2019). Analysis on dynamics characteristics of vibratory harvesting for oil-tea Camellia fruit. Paper presented at the *2019 ASABE Annual International Meeting*, Boston, Massachusetts, July 7–10.

[2] Dong, W., Wu, Y., Liu, F., Hu, H., Yan, J., Bai, H., & Zhao, X. (2024). Design and experiment of a harvesting header for wide–narrow-row corn. *Applied Sciences*, 14(3), Article 1309. https://doi.org/10.3390/app14031309

[3] Fu, J., Zhang, M., Cheng, C., Zhao, H., & Ren, L. (2024). Thickness monitoring of threshing mixture on the oscillating plate of corn grain harvester. *Computers and Electronics agriculture*, 227, 109485. https://doi.org/10.1016/j.compag.2024.109485

[4] Fu, L., Peng, J., Nan, Q., He, D., Yang, Y., & Cui, Y. (2016). Simulation of vibration harvesting mechanism for sea buckthorn. *Engineering in Agriculture, Environment and Food*, 9(1), 10-108. https://doi.org/10.1016/j.eaef.2015.08.003

[5] Fu, Q., Fu, J., Chen, Z., & Ren, L. (2020). Analysis and experiment on the mechanism of rigid-flexible coupling loss reduction of corn ear-picking header (玉米摘穗割台刚柔耦合减损机理分析与试验). *Transactions of the Chinese Society of Agricultural Machinery*, 51(4), 60–68.

[6] Geng, D., Li, Y., Meng, F., Meng, P., Ni, G., & Zhang, M. (2017). Design and experiment of multi-sided vertical roller ear picking device for corn harvester (玉米收获机多棱立辊式摘穗装置设计与试验). *Transactions of the Chinese Society of Agricultural Machinery*, 48(3), 84–91.

[7] Geng, D., Wang, Q., Lu, X., Yu, X., Liu, Y., & Jin, C. (2019). Design and experiment of corn multi-ribbed ear picking roller based on excitation theory (基于激振理论的玉米多棱摘穗辊设计与试验). *Transactions of the Chinese Society of Agricultural Machinery*, 50(5), 124–132.

[8] Ji, X., Geng, D., Yao, Y., Du, J., Zhu, J., & Xu, H. (2020). Design and experiment of vibration ear-picking device for corn harvester (玉米收获机激振摘穗装置设计与试验). *Transactions of the Chinese Society of Agricultural Machinery*, 51(S2), 126–133.

[9] Liu, F. (2007). Research on key components of vertical ear-removing roller corn harvester for harvesting both ears and stems [Master's thesis, Jilin University].

[10] Pereira, M. R., Santos, F.L., Scinocca, F., Tinoco, H. A., & Villibor, G.P. (2025). Evaluation of the transmissibility of vibration and dynamic behaviour of coffee plants under field conditions. *Biosystems Engineering*, 250, 225–235. https://doi.org/10.1016/j.biosystemseng.2025.01.002

[11] Wang, Q., He, K., Jin, C., Lu, X., Geng, D., & Zhang, G. (2018). Analysis on the mechanism of corn vibration ear picking and optimization of parameter experiments (玉米激振摘穗机理分析与参数试验优化). *Transactions of the Chinese Society of Agricultural Machinery*, 49(S1), 249–257.

[12] Wang, Q., He, Q., Yue, D., Li, D., Yin, J., Guan, P., & Wang, Z. (2025). Dynamic real-time detection for corn kernel breakage rate based on deep learning and sliding window technology. *Computers and Electronics in Agriculture*, 232, 109926. https://doi.org/10.1016/j.compag.2025.109926

[13] Wu, D., Zhao, E., Fang, D., Jiang, S., Wu, C., Wang, W., & Wang, R. (2022). Determination of vibration picking parameters of Camellia oleifera fruit based on acceleration and strain response of branches. *Agriculture*, 12(8), Article 1222. https://doi.org/10.3390/agriculture12081222

[14] Xing, S., Cui, T., Zhang, D., Yang, L., He, X., Li, C., & Du, Z. (2024). Design and optimization for a longitudinal-flow corn ear threshing device of low loss and low energy consumption. *Computers and Electronics in Agriculture*, 226, 109328. https://doi.org/10.1016/j.compag.2024.109328

[15] Xing, S., Cui, T., Zhang, D., Yang, L., He, X., Wang, Z., & Jing, M. (2024). Design and experiment of the simulated electronic corn ear based on UWB/IMU technology. *Computers and Electronics in Agriculture*, 217, 108567. https://doi.org/10.1016/j.compag.2023.108567

[16] Xuan, Y., Xu, L., Liu, G., & Zhou, J. (2021). The potential influence of tree crown structure on the ginkgo harvest. *Forests*, 12(3), Article 366. https://doi.org/10.3390/f12030366

[17] Xin, S., Zhao, W., Shi, L., Dai, F., Feng, B., Yan, Z., & Lü, D. (2023). Design and experiment of the clamping and conveying device of the vertical roller corn harvesting header (立辊式玉米收获割台夹持输送装置设计与试验). *Transactions of the Chinese Society of Agricultural Engineering*, 39(9), 34–43.

[18] Yan, H., Wu, W., Han, F., & Liu, F. (2009). Effect of the roller type of corn harvester's ear picking roller on its working performance (立辊型玉米收获机摘穗辊辊型对工作性能的影响). *Transactions of the Chinese Society of Agricultural Machinery*, 40(5), 76–80.

[19] Yang, R., Chen, D., Zha, X., Pan, Z., & Shang, S. (2021). Optimization design and experiment of ear-picking and threshing devices of corn plot kernel harvester. *Agriculture*, 11(9), Article 904. https://doi.org/10.3390/agriculture11090904

[20] Zhao, J., Ma, T., Inagaki, T., Chen, Q., Gao, Z., Sun, L., & Chen, J. (2021). Finite element method simulations and experiments of detachments of Lycium barbarum L. *Forests*, 12(6), Article 699. https://doi.org/10.3390/f12060699

[21] Zhao, J., Tsuchikawa, S., Ma, T., Hu, G., Chen, Y., Wang, Z., & Chen, J. (2021). Modal analysis and experiment of a *Lycium barbarum L*. shrub for efficient vibration harvesting of fruit. *Agriculture*, 11(6), Article 519. https://doi.org/10.3390/agriculture11060519

[22] Zheng, Z., Hu, Y., Dong, J., Zhao, P., Liu, Y., Jiang, X., & Huang, Y. (2024). Characterising vibration patterns of winter jujube trees to optimise automated fruit harvesting. *Biosystems Engineering*, 248, 255–268. https://doi.org/10.1016/j.biosystemseng.2024.11.004

[23] Zhuo, P., Li, Y., Wang, B., Jiao, H., Wang, P., Li, C., & Wang, L. (2022). Analysis and experimental study on vibration response characteristics of mechanical harvesting of jujube. *Computers and Electronics in Agriculture*, 203, 107446. https://doi.org/10.1016/j.compag.2022.107446